Biochimica et Biophysica Acta 1838 (2014) 1777–1784

Contents lists available at ScienceDirect

Biochimica et Biophysica Acta

journal homepage: www.elsevier.com/locate/bbamem

A conserved tetrameric interaction of cry toxin helix α3 suggests a functional role for toxin oligomerization

Xin Lin [1], Krupakar Parthasarathy [1], Wahyu Surya, Tong Zhang, Yuguang Mu, Jaume Torres *

School of Biological Sciences, Nanyang Technological University, 60, Nanyang Drive, 637551, Singapore

ARTICLE INFO

Article history:
Received 3 January 2014
Received in revised form 10 March 2014
Accepted 14 March 2014
Available online 20 March 2014

Keywords:
Cry toxin
Oligomerization
Coiled-coil
Evolutionary conservation
Membrane insertion

ABSTRACT

Crystal (Cry) toxins are widely used for insect control, but their mechanism of toxicity is still uncertain. These toxins can form lytic pores in vitro, and water soluble tetrameric pre-pore intermediates have been reported. Even the precise oligomeric state of the toxin in membranes, trimeric or tetrameric, is still a debated issue. Based on previous reports, we have assumed that interactions between toxin monomers in solution are at least partly mediated by domain I, and we have analyzed in silico the homo-oligomerization tendencies of the domain I α-helices individually. Using many homologous sequences for each α-helix, our strategy allows selection of evolutionarily conserved interactions. These interactions appeared only in helices α3 and α5, but only α3 produced a suitably oriented or α-helical sample in lipid bilayers, forming homotetramers in C14-betaine, and allowing determination of its rotational orientation in lipid bilayers using site-specific infrared dichroism (SSID). The determined orientation in the tetrameric model is in agreement with only one of the evolutionarily conserved models. In addition mutation R99E, which was found to inhibit oligomerization experimentally, greatly destabilized the tetramer in molecular dynamic simulations. In this model, helix 3 is able to form inter-monomer interactions without significant rearrangements of domain I, which is compatible with the available crystal structure of Cry toxins in solution. The model presented here at least partially explains the reported tetrameric oligomerization of Cry toxins in solution and the inhibition of this oligomerization by a synthetic α3 peptide.

1. Introduction

The crystal (Cry) insecticidal toxins, or δ-endotoxins, are produced by the Gram positive soil bacterium *Bacillus thuringiensis* (Bt). These proteins are arranged in different classes [1] and are toxic to a wide variety of insect larvae of the orders Coleoptera, Diptera and Lepidoptera [2], having also a high specificity. For this reason, and since they are safe for the environment, they are widely used as a biopesticide [3]. The three-dimensional structure of several Cry toxins has revealed a similar three-domain arrangement [4–6]. Domain I has been suggested to be a pore-forming domain [7–9] comprising seven α-helices, named α1–α7. Domains II and III, composed of β-sheets, are responsible for binding specificity and structural integrity [10].

The mechanism of action of Cry toxins takes place in several steps (see [11], for a recent review). Briefly, the crystal is solubilized in the highly alkaline insect midgut lumen. Then, the toxins are activated proteolytically by intestinal proteases. These activated toxins are able to bind to specific receptors on the midgut brush border membrane (BBM) surface. After binding, it has been proposed that the toxin undergoes a conformational change and inserts in the membrane, leading to pore formation and cell lysis [12,13].

An alternative mechanism [14] has been suggested after observing the effect of Cry1Ab toxin in non-susceptible insect cells that expressed the *Manduca sexta* Cry1Ab toxin receptor, Bt-R_1: upon Cry toxin binding to that receptor, a signal pathway is activated, which involves stimulation of G protein and adenylyl cyclase, amongst others, leading to cell death.

A striking difference between these two mechanisms is the role of Cry oligomerization: whereas in the alternative model [14] only monomers were found to be relevant for toxicity, in the pore-forming model a water-soluble pre-pore intermediate has been postulated. Indeed, after incubation of the toxin with a peptide that mimics the cadherin receptor, tetrameric oligomers were observed, which were suggested to constitute the pore-forming unit [15–17]. These tetramers were more active than the monomeric form, both in insertion and in pore formation. More recent studies using single molecule fluorescence have shown that in lipid bilayers *B. thuringiensis* Cry1Aa forms oligomers when incorporated to lipid bilayers up to the level of tetramer, although the presence of substantial amounts of trimers in the membranes could not be discarded even at high toxin concentration [18].

* Corresponding author. Tel.: +65 6316 2857; fax: +65 6791 3856.
E-mail address: jtorres@ntu.edu.sg (J. Torres).
[1] These authors have contributed equally.

http://dx.doi.org/10.1016/j.bbamem.2014.03.006
0005-2736/

It has been reported that a synthetic peptide corresponding to the α3 helix of domain I in Cry1Ab prevents pre-pore tetramer formation, whereas synthetic peptides corresponding to the other helices in domain I did not have any effect in oligomerization [19]. This inhibitory effect of α3 was attributed to competition of α3 peptide for the monomer–monomer interfaces in the homo-tetramer. This is consistent with the accessible position of helix α3 in the domain I of the water soluble form of Cry toxins, e.g., [4,20]. In these structures, helices 1, 2, 3, 4 and 6 surround helices 5 and 7 (Fig. 1A), the latter being in contact with domains II and II. A predicted coiled-coil propensity in helix α3 [19], led the authors to suggest that positions *a* and *d* (Fig. 1) in a hypothetic coiled-coil *a-b-c-d-e-f-g* repeat were involved in pre-pore tetramer formation, i.e., in establishing the necessary contacts between Cry monomers.

However, in the available crystal structures of Cry toxins, e.g., δ-endotoxin Cry3A [20], positions *a* and *d* are involved in interactions with helices of the same monomer, specifically with domain I helix α5. Therefore, the proposition that positions *a* and *d* participate in inter-monomer interactions would require a dramatic rearrangement of the α3 helix, with a rotation of approximately 180°. Indeed, most mutations at positions *a* and *d* obtained to test the disruption of oligomerization led to destabilization of the monomeric toxin [19], preventing further investigation. This is expected from their orientation in the crystal structure, facing α5. Of those that were stable, i.e., Y107E and L100E (Fig. 1B, *a* positions), Y107E impaired both pre-pore oligomerization and toxicity as expected from the hypothesis, but L100E conserved toxicity. In addition, mutations at positions other than *a* or *d*, e.g., position *g* R99 [21], also impaired pore formation. These results therefore were inconsistent with the hypothesis presented in terms of the orientation of the α3 helix. However, if helix α3 prevents oligomerization, it still may do so via interactions through the opposite face, i.e., positions *b-f-c* (Fig. 1A, broken line), which are solvent exposed in the crystal structure of domain I.

In the present paper, using a computational approach [22], we have first sought to determine the predisposition of each one of the α-helices in domain I of Cry toxins to form homomeric interactions. In this approach, which we have applied previously to successfully predict the homo-oligomeric association of various transmembrane (TM) α-helical domains [23–28], non valid models are filtered out by performing independently the same simulation for a list of homologous sequences that are likely to share the same backbone structure and oligomeric size. The rationale is that multiple sequence variations present in these sequences will eventually destabilize models that are not present in vivo, but will preserve at least the native one, which will appear as a stable structure simultaneously in the simulations of all sequences tested. Such preserved model is referred to as a 'complete set', and is considered to represent a candidate for a native interaction. In the simulations, we have used a dielectric constant of 80 and 1, to represent interactions in solution and in the membrane, respectively. The likelihood of the models obtained has been independently assessed using biophysical assays of these α-helical domains.

2. Materials and methods

2.1. Molecular dynamics simulations—global search

Simulations were performed using a Compaq Alpha Cluster SC45 which contains 47 nodes, and calculations were carried out using the parallel version of the *Crystallography and NMR System* (CNS Version 0.3, PCNS) [29], as described elsewhere [30]. The protocol for the global search and clustering of structures has been described previously [22, 24,25]. Briefly, the global search was carried out in vacuo with united atoms, explicitly describing only polar and aromatic hydrogen atoms using CHI 1.1 (*CNS Helical Interactions*). As the models tested are homooligomers, the interaction between the helices was assumed to be symmetrical.

Trials were carried out starting from either left or right crossing angle configurations. The initial helix tilt, β, was restrained to 0° and the helices were rotated about their long helical axes in 10° increments until the rotation angle reached 350°. Henceforth, the simulation was repeated by increasing the helix tilt in discrete steps of 5°, up to 45°. Three trials were carried out for each starting configuration using different initial random velocities.

Clusters were identified with a minimum number of eight similar structures. Any structure belonging to a certain cluster was within 1.5 Å RMSD (*root mean square deviation*) from any other structure within the same cluster. Finally, the structures belonging to each cluster were averaged and subjected to energy minimization. These final averaged structures, described by a certain tilt and rotational orientation at a specified arbitrary residue, were taken as the representatives of the respective clusters. The tilt angle, β, of the models was taken as the average of the angles between the bundle axis and each helix axis in the bundle. The bundle axis, coincident with the normal to the bilayer, was calculated by CHI. The helix axis was calculated as a vector with starting and end points above and below a defined residue, where the points correspond to the geometric mean of the coordinates of the five

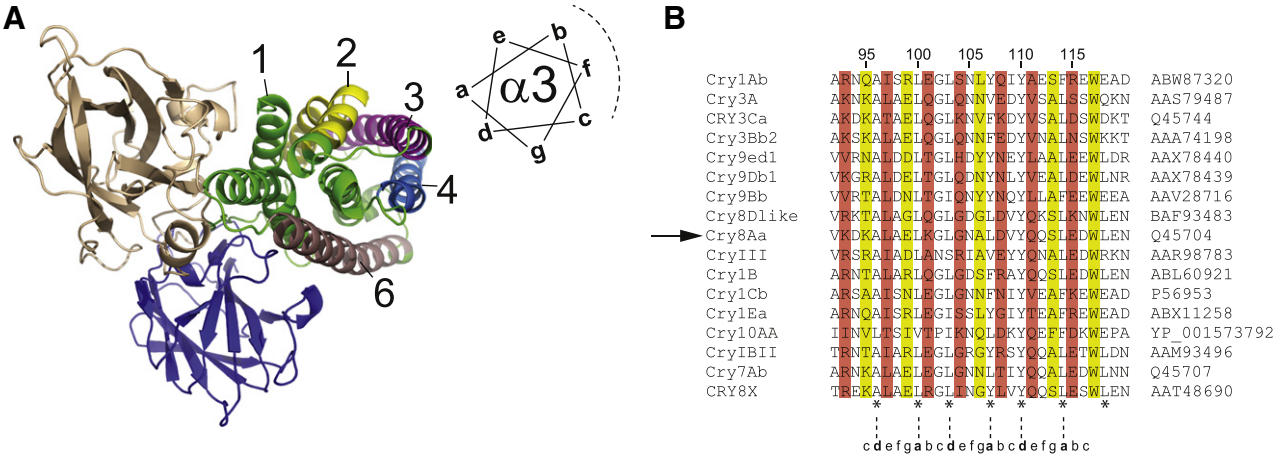

Fig. 1. (A) Crystal structure of Cry3a [20] with helices 1 to 6 indicated, and distribution of positions *a–g* in a helical wheel for helix α3 (the broken line indicates the solvent exposed face); (B) Alignment of 17 sequences used in the MD simulation corresponding to the α3 helix in Cry toxin homologs. Residue numbers correspond to the Cry1Ab sequence. Accession numbers are indicated on the right. In this alignment, residues labeled with a star (a and d) face the interior of domain I in the crystal structure [20]. The arrow shows the sequence of the peptide synthesized.

α carbons N-terminal and the five α carbons C-terminal to the defined residue. The rotational orientation angle ω of a residue is defined by the angle between a vector perpendicular to the helix axis, oriented towards the middle of the peptidic C═O bond of the residue, and a plane that contains both the helical axis and the normal to the bilayer. Inter-sequence comparisons between low energy clusters were performed by calculating the RMSD between their α-carbon backbone. Fitting was performed using the program ProFit (http://www.bioinf.org.uk/software/profit). The energies calculated corresponded to the total energy of the system, including both bonded and non-bonded, e.g., bond, angle, dihedral, improper, and Van der Waals and electrostatic terms, respectively [30]. The interaction energy for the residues was calculated with the function *chi_interaction* implemented in CHI.

To find the possible oligomeric state and mode of interaction, simulations were performed with 17 homologous sequences of each α-helix in Cry toxin domain I, obtained from the National Center for Biotechnology Information (NCBI). For each sequence, three trials were carried out for each starting configuration using different initial random velocities, testing right and left-handed configurations, from dimers to pentamers, and producing 51,840 structures for each helix-sequence. The correct model amongst all these candidates has to be determined using complementary experimental data, e.g., site specific infrared dichroism, NMR or crystallography. A complementary alternative is to perform these simulations, not only for one sequence, but also for its homologues [22,31], as these are supposed to share the same backbone structure.

Sequences used in the simulations for Cry3a were GALVS…EQVEA (α2), AKNKA…SWQKN (α3), DIAEF…WYNV (α6) and SWVNF…ALFP (α7), whereas the corresponding sequences for other homologs were simply those obtained after alignment. Only those corresponding to α3 are shown (Fig. 1B). The results for sequences α4 and α5 have been reported previously [32], whereas helix α1 in Cry3a is only ~15 residues long, and it is cleaved after binding to receptors [16]; therefore, it was not included in the analysis.

2.2. Molecular dynamics simulations—stability of helix α3 mutant R99E in the tetrameric model 3

The tetrameric model 3 formed by α3 peptide from Cry8Aa, parameterized by the AMBER03d force field, was taken as the initial structure for simulations with both wild type (WT) and R99E mutant. In both simulations, the tetramer was initially placed in the center of a rectangular box with a volume of 89.45 nm^3, followed by addition of 2279 and 2281 TIP3P water molecules [33] into the box for WT and R99E, respectively. Counter ions were added to the box for WT to make the system neutral. The pH was set to 7 with Arg and Lys residues positively charged, and the Glu and Asp residues negatively charged. GROMACS (version 4.5) software package was used to perform both simulations [34] The LINCS protocol [35] was used to constrain the bonds involving hydrogen atoms, allowing an integration time step of 2 fs. The particle mesh Ewald method [36] with a cutoff of 1.0 nm was used to treat the electrostatic interactions. A cutoff of 1.2 nm was used for the van der Waals interactions. The non-bonded pair lists were updated every 0.010 ps. The coordinates were saved every 2 ps. Temperature, 300 K, was controlled by the Bussi–Donadio–Parrinello velocity rescaling thermostat found to sample the canonical ensemble [37]. Both simulations ran for 50 ns.

2.3. Accessibility momentum calculation

The percentage of accessible surface of each residue was calculated using MolMol [38]. Thus, for each residue, accessibility was represented by the length of a vector directed outwards from the center of the helix towards the α-carbon of the corresponding residue. Vectors for all residues were added to obtain the total accessibility momentum of the helix, which should point towards its most solvent-accessible face. The three terminal residues at each end of the peptide were not included in the calculation, as these residues are exposed to solvent.

2.4. Peptide synthesis and purification

Peptides were synthesized using 9-fluorenyl-methyloxycarbonyl (FMOC) solid-phase chemistry (Liberty Microwave Peptide Synthesizer, CEM, NC, USA) and Tentagel amide resin (Intavis AG, Germany). The peptides were cleaved from the resin with trifluoroacetic acid (TFA). The lyophilized peptides were dissolved in acetonitrile, injected into a C18 HPLC column, and eluted in a linear gradient of water/acetonitrile, from 0% to 100% acetonitrile. Peptide purity was confirmed by electrospray ionization (ESI) mass spectrometry. The purified peptides were lyophilized overnight after addition of 10 mM HCl, to remove possible TFA adducts.

2.5. $^{16}O/^{18}O$ exchange

To introduce the isotopically labeled amino acids, commercially available $^{13}C{=}^{16}O$ labeled amino acids (Cambridge Isotopes Laboratories, Andover, MA) A and L were exchanged to a double isotope, $^{13}C{=}^{18}O$, by incubating the amino acid at 100 °C at acidic pH conditions (pH ~1) with a mixture of $H_2^{18}O$ and dioxane (3:1, *v*/*v*) for 1 h, as described previously [39]. The extent of exchange was monitored using mass spectrometry. The solution was lyophilized and the amino acid was derivatized with FMOC [40].

2.6. Sequence and isotopic labeling

Orientation determination by site specific infrared dichroism SSID [41] requires both α-helical conformation and order, and the latter can be obtained if the peptide inserts in lipid bilayers. To confirm the rotational orientation obtained from the in silico analysis, the peptide corresponding to helix α3 was taken from Cry8Aa (Fig. 1B, arrow) because it showed the highest α-helical propensity, according to the consensus predicted secondary structure from a set of twelve algorithms [42]. Two differently labeled peptides were synthesized for this sequence, each containing one $^{13}C{=}^{18}O$ -labeled carbonyl, one at A144 and another at L145, equivalent to positions A106 and L107 in Cry1Ab (V_{130}KDKALAELKG LGNALDVYQQ SLEDWLEN$_{158}$ (labeled residues underlined).

We also attempted to confirm the orientation of α5 helix reported in [32] by synthesizing the α5 peptide. We used initially the sequence Cry4Ba sequence ELLLLPIYAQ VANENLLLIR DGLINAQEWSL. However, this peptide produced a low dichroism in the infrared spectra both for amide I and A bands (not shown), indicative of either low order or a not completely α-helical sample. In an attempt to obtain a more ordered peptide, we synthesized α5 from Cry1Ba2: LLMVYAQAAN LHLLLLRDAS LFG (23 residues) and QEVPLLMVYA QAANLHLLLL RDASLFGSEF (30 residues). The first of these showed at least 50% of β-structure, whereas the second was more α-helical, but the order parameter was still negative. Lastly, we also synthesized a peptide encompassing α4 and α5 (Q_{140}SYRT…NAQEW$_{199}$). However, none of these peptides produced a sample suitable for SSID in lipid bilayers.

2.7. Circular dichroism (CD)

CD spectra were measured on a Chirascan CD Spectrometer (Applied Photophysics, UK). Data were collected at 20 °C at 1 nm interval, from 190 nm to 240 nm, on a 1 mm pathlength cell, in 50 mM Tris, 100 mM NaCl, pH 7.3. The peptide concentration was 50 μM. The peptide was first dissolved in HFIP and dried, followed by resuspension in the solution. When measuring the spectrum in the presence of detergent, final detergent concentration was 5 mM C-14 Betaine (cmc 100 μM). Spectra were smoothed with a Salvitsky–Golay algorithm.

2.8. Analytical ultracentrifugation

Preliminary CD and AUC results indicated that in aqueous solution the α3 peptide was found to adopt a random coil conformation and no oligomers; therefore, AUC was performed in the presence of detergents. Sedimentation equilibrium experiments were performed using a Beckman XL-I analytical ultracentrifuge at 25 °C [43]. Absorbance was measured at 250 nm ($\varepsilon_{250} = 4367\ M^{-1}\ cm^{-1}$). The buffer composition was 50 mM Tris, 100 mM NaCl, pH 7.3 and 5 mM C14 Betaine. To match the density of the detergent, D_2O was added to the buffer to a final volume ratio of 29.4% [44]. The monomeric molecular mass of the α3 peptide and its partial specific volume were calculated with the program SEDNTERP [45]. The monomeric mass of the peptide was determined to be 3265 Da, whereas the partial specific volume, calculated after correction for partial hydrogen/deuterium exchange [43], was 0.7421 cm^3/g at 25 °C. The density-matched buffer was added to the dry peptide. The concentration of detergent was 5 mM in all cells, and the peptide:detergent molar ratio was 1:25, 1:50 and 1:100 for inner, medium and outer cells, respectively. The samples were centrifuged in three-compartment carbon-epoxy centerpieces with quartz windows for lengths of time sufficient to achieve equilibrium, tested with the software WinMatch. Equilibrium was typically achieved after 26 h for each speed: 30 K, 40 K and 48 K rpm. The equilibrium data sets were processed and analyzed using the programs Sedfit and Sedphat [46]. At the end of each run, absorbance data at 250 nm was obtained.

2.9. Infrared spectroscopy

Infrared spectra were acquired on a Nicolet Nexus spectrometer (Madison, USA) purged with N_2 and equipped with an MCT/A detector cooled with liquid nitrogen. Attenuated total reflection (ATR) spectra were collected with a 25-reflection ATR accessory from Graseby Specac (Kent, UK) and a wire grid polarizer (0.25 μm, Graseby, Specac). A total of 200 interferograms collected at a resolution of 4 cm^{-1} were processed with 1 point zero filling and Happ–Genzel apodization. The purified peptide was incorporated in multilamellar liposomes by first dissolving a dry mixture of lipid and lyophilized peptide (50:1 molar ratio) in HFIP. The solution was dried by a stream of N_2, and the resulting peptide-lipid film was dissolved in phosphate buffer (1 mM, pH 7) followed by sonication. The DMPC liposome solution was deposited on a germanium internal reflection element (IRE) and dried slowly by evaporation. Hydrogen/deuterium (H/D) exchange was performed by flowing D_2O-saturated nitrogen into the ATR chamber for a few hours. Amide proton H/D exchange was detected from the reduction in intensity of amide A and II bands in the non-polarized spectra, which were obtained from parallel (∥) and perpendicular (⊥) ATR polarized spectra, using the expression 1(∥) + 1.44(⊥) [47]. Dichroic ratios and percentage of H/D exchange were calculated as described previously [48] and helix rotational orientation was calculated as described using SSID [41]. Order parameters were calculated essentially as described [49].

3. Results and discussion

First, we performed molecular dynamic (MD) simulations to obtain candidate models for homo-oligomerization. For each helix, 17 homologs were used in order to test for evolutionary conservation of the inter-helical interactions (see Materials and methods) as described previously [22]. No 'complete set' was obtained from homo-dimeric to homo-pentameric arrangements, at any helix tilt or rotational orientation tested, for α2, α6 or α7 helices (not shown). For α4 and α5, in a previous report [32] we could only find a conserved homotrimer for α5, but no model for α4 [32]. These results are consistent with the lack of effect on oligomerization by mutations at helix α6 [19] and α4 in Cry1Ab [50]. For helix α3, in contrast, we found four 'complete sets', i.e., conserved models; two trimers and two tetramers, where the accessibility moment, i.e., the most solvent-accessible side, is represented by a vector (Fig. 2A). These vectors should point towards the interior of domain I in the crystal structure if Cry toxin monomer–monomer interaction via α3 does not involve any large conformational change. As shown in Fig. 2B, this condition is only satisfied by models 2 (trimer) and 3 (tetramer). Similarly, it is difficult to rationalize α5-mediated interactions in solution, as this helix is embedded in domain I and not accessible to solvent.

Nevertheless, to confirm the type of oligomer, if any, formed by α3 and α5 helices, we synthesized these peptides. The interaction between Cry toxin monomers in solution is supposed to take place in the context of a complete domain I; therefore, a synthetic peptide corresponding to one of its α-helices may not be α-helical in aqueous solution. Indeed, we found that this was the case for the peptides corresponding to helix α3 and α5. Peptide α3 was soluble in water but it was not α-helical (Fig. 3). When this peptide was analyzed by equilibrium sedimentation in water, the sedimentation profile was consistent with the presence of only monomers, as the absorbance profile was featureless (not shown). However, when this peptide was solubilized in detergent, CD experiments indicated that it was α-helical (Fig. 3), later confirmed by FTIR (see below). Thus, equilibrium sedimentation experiments of α3 were performed in the detergent C14-betaine (Fig. 4A–B). The best fit to the data was obtained with a monomer: *n*-mer reversible equilibrium, where $n = 4$ (i.e., tetrameric) (Fig. 4C–D) and $K_a = 5 \times 10^{10}\ M^{-3}$, or $3.6 \times 10^3\ M^{-1}$, i.e., a K_d for monomer–monomer interaction of approximately 0.3 mM.

It has been shown previously that inter-helical interactions in a detergent environment are weaker than in lipid bilayers [51]. Thus it is reasonable to assume that peptide α3 also forms oligomers in lipid bilayers, and that these oligomers are also tetrameric. We note that a tetrameric interaction has been proposed previously when the toxin is inserted in membranes, on the basis of single molecule fluorescence [18] and as a pre-pore intermediate [19].

The fact that the peptide α3 is α-helical and forms oligomers in a detergent environment, provides the opportunity to investigate its

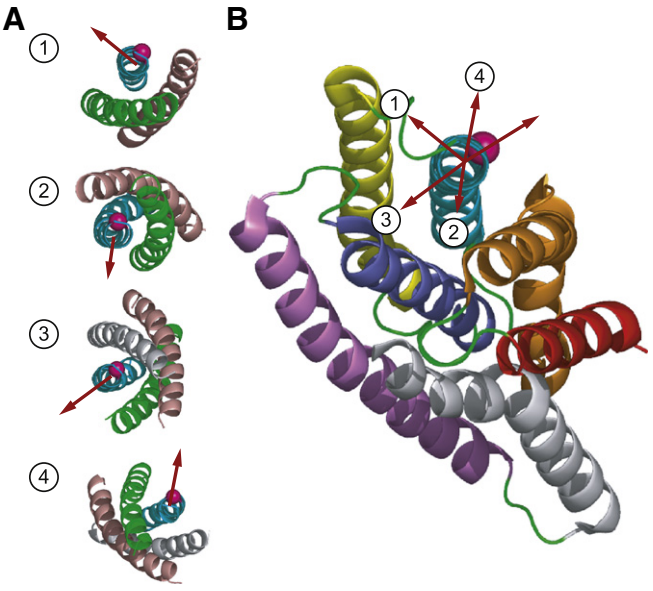

Fig. 2. Accessibility momenta for the four evolutionarily conserved models (1–4) relative to domain I. (A), The four evolutionary conserved α3 homomeric models resulting from our simulation; the direction of the accessibility momentum is indicated by an arrow. As a reference, the α-carbon atom of S151 in helix α3 is shown as a pink sphere; (B), ribbon representation of the crystal structure of domain I in Cry3A, with helices α1 (red), α2 (orange), α3 (light blue), α4 (yellow), α5 (dark blue), α6 (purple) and α7 (grey). The four accessibility momenta in (A) (arrows labeled 1–4) are superimposed on the α3 helix in domain I, along with the accessibility vector of helix α3 in domain I (arrow unnumbered), which indicates its most accessible side.

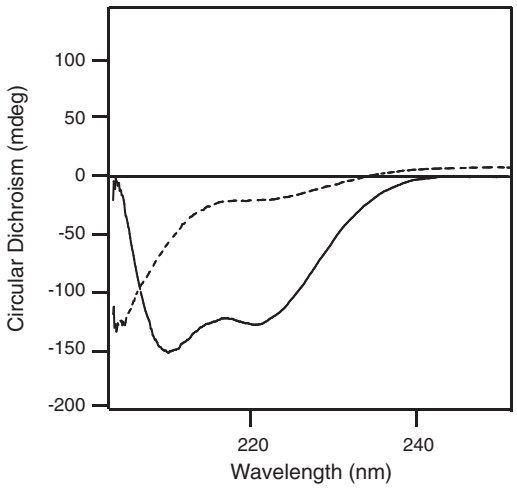

Fig. 3. Circular dichroism results corresponding to the synthetic peptide α3 in aqueous solution (broken line) or in C14-betaine detergent micelles (solid line).

rotational orientation in model planar lipid bilayers, provided that the peptide inserts in membranes in an orientation almost perpendicular to the membrane plane, as is expected for homo-oligomers [41]. We note that this was not the case for a Cry3Aa α3 peptide [49], which was claimed to adopt an orientation parallel to the membrane surface, although in that work only the amide I infrared spectrum of one peptide, that of α2, was explicitly shown. In our hands, however, α3 peptide from Cry8Aa was α-helical in lipid bilayers and was properly inserted in the membrane (see below). This allowed determination of the rotational orientation of this peptide using site specific infrared dichroism (SSID) [41]. We measured the orientation of two consecutive isotopically-labeled peptidic carbonyl bonds (C═O), at A144 and at L145, by determination of the dichroisms of the amide A (N–H_s), amide I (C═O_s) and (C═O_s) (Fig. 5A), using two independent measurements for each labeled peptide. For the peptide labeled at amino acid A144, the values for amide A, amide I and labeled carbonyl dichroisms were respectively (2.5, 2.4, 2) and (2.2, 2.1, 1.8). For the second peptide, labeled at L145, these values were (2.4, 2.1, 2.4) and (2.3, 2.0, 2.2). Combining these dichroisms, the rotational orientation of A144 was found to be 180° ± 17°, whereas the average α3 helix tilt from the membrane normal was 24° ± 6°.

The rotational orientations of the equivalent residue A144 in models 1–4 (Fig. 2A) were determined to be 118°, 59°, 189° and 91°, respectively. Thus, the only compatible model with our experimental measurement by SSID (180° ± 17°) is model 3, which also satisfies our experimental observations in terms of oligomeric size (tetrameric). Further, in model 3, residues at positions labeled *a* and *d* are solvent exposed, i.e., in the absence of structural rearrangements in the context of a complete domain I, they would face helix α5 (Fig. 1A). That is, only in model 3 the accessibility vector (Fig. 2B) coincides with the most buried face of α3 in domain I. In turn, the positions *b-c-f* in model 3, which face the other α3 helices in the homotetramer, in the context of a complete domain I would be exposed to solvent and therefore available for domain I monomer–monomer interactions without significant domain I conformational change. Mutation R99E in helix α3 of Cry1Aa was found to be a strong inhibitor of oligomerization [19,50]. This residue is at position *g* (Fig. 1), and it is involved in inter-monomer interactions in our model 3 (Fig. 5B–C) consistent with available mutagenesis data. In contrast, in the other tetrameric model, this residue is facing the interior of the tetrameric bundle (not shown). To test if this mutation is really critical for the stability of model 3, we performed a molecular dynamics simulation (Fig. 6). For the WT peptide, 11 clusters were found in total, and the largest cluster was 72.8% of the population. For mutant R99E, 61 clusters were found, and the largest cluster was only 14.8% of the population. While the RMSD did not change for the WT peptide, the stability of the tetramer was seriously compromised by the presence of the mutation, showing an increase from 0.3 to 1.1 in 35 ns (Fig. 6A). The initial and final models in these simulations are shown in the same figure for WT and mutant peptide (Fig. 6B–C).

Tetrameric model 3 for α3 helix interaction thus represents at least part of the interactions between monomers that take place when the complete toxin is still in solution. However, the fact that the present

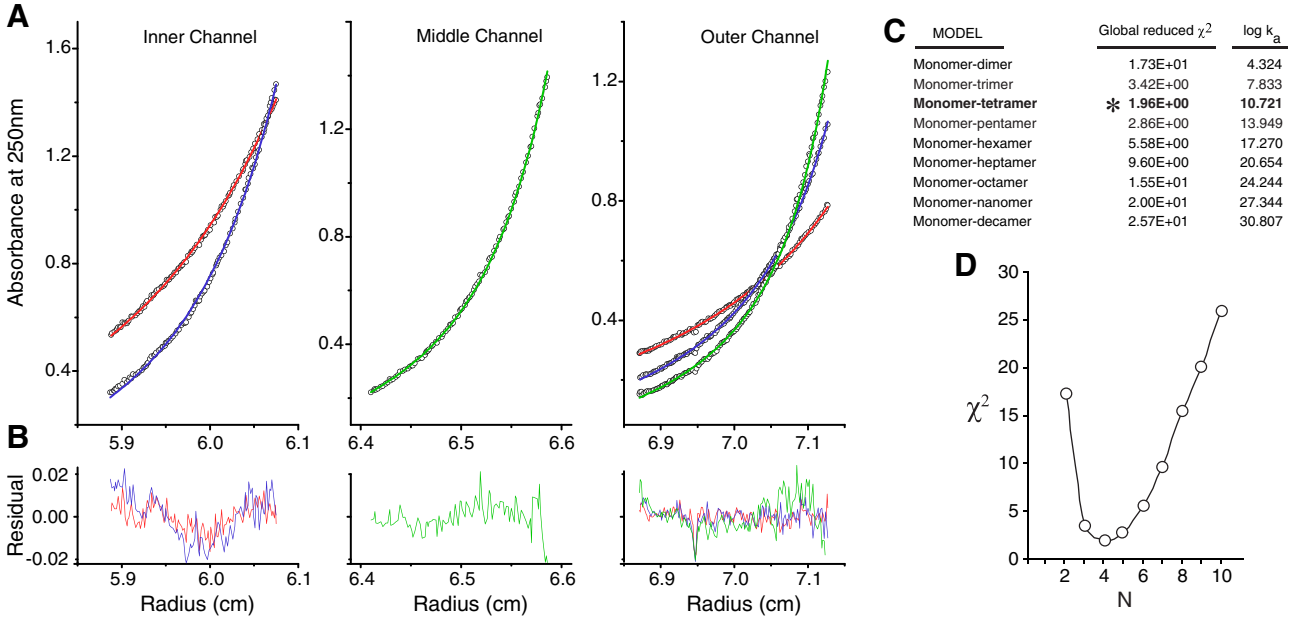

Fig. 4. Sedimentation equilibrium results for Cry α3-peptide in C-14 Betaine micelles. (A) Inner, medium and outer cells, at the following peptide:detergent molar ratios: 1:50, 1:37, 1:25 at 48,000 rpm (green), 40,000 rpm (blue) and 30,000 rpm (red). The data was best fitted to a monomer-tetramer equilibrium model; (B) residuals of the fitting; (C) association constant values for each of the models tested; (D) Graphical representation of the χ2 of each of the models. The curves that are absent in (A) were deemed unsuitable for fitting and were not included in the fit.

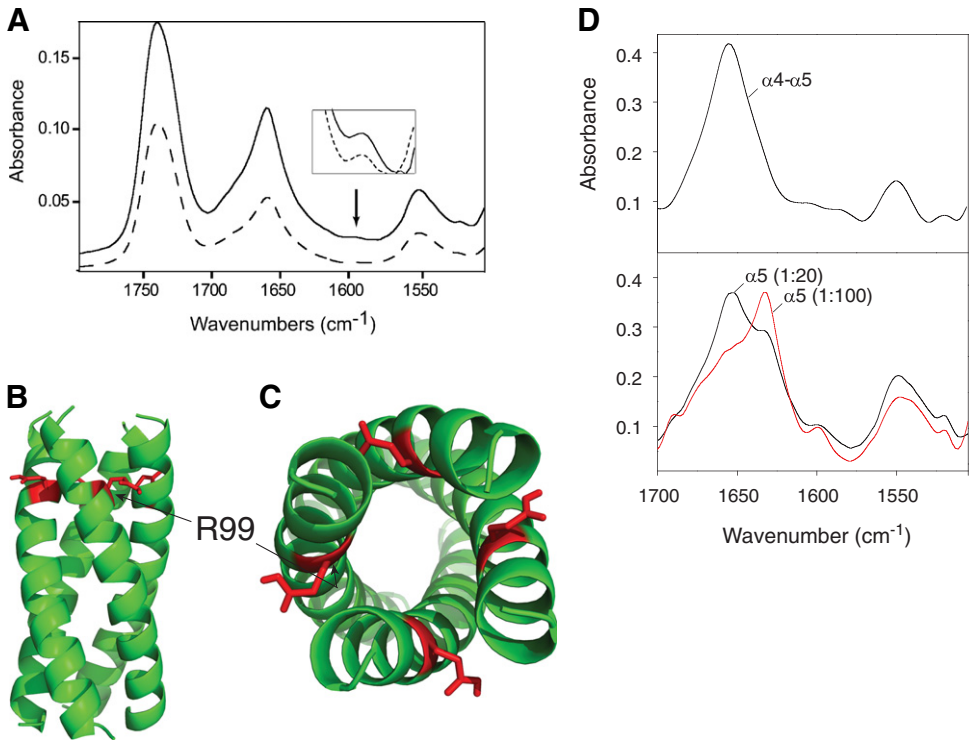

Fig. 5. (A) ATR FTIR spectra of the synthetic Cry α3 peptide reconstituted in DMPC bilayers. The spectra show the Amide I (1700–1600 cm^{-1}) region corresponding to the 0° (continuous line) and 90° polarizations (broken line). The arrow indicates the band due to the isotopic label ($^{13}C{=}{=}^{18}O$). For clarity, the band corresponding to the label is enlarged and shown in the insert; (B–C) Side and top views of the tetrameric model 3 in agreement with the SSID orientation of the α3 peptide in lipid bilayers. The interfacial position of the residue Arg99 in Cry1Ab (equivalent to Glu in Cry8Aa, see Fig. 1B) is indicated; (D), spectra corresponding to synthetic Cry4Ba α4–α5 peptide (top) and α5 (bottom) in DMPC at a P/L ratio 1:20, except for one of the spectra of α5 at 1:100.

data was obtained in membranes suggests that the membrane embedded form of the toxin also may use this interaction.

The fact that the peptide α3 was α-helical in detergent micelles and in lipid membranes allowed determination of orientation by SSID, but this was not possible for helix α5, the other helix for which we found an evolutionarily conserved model [32]. We synthesized a peptide corresponding to Cry4Ba α5, and also a peptide spanning both helices α4 and α5 (see Materials and methods section). However, α5 had the

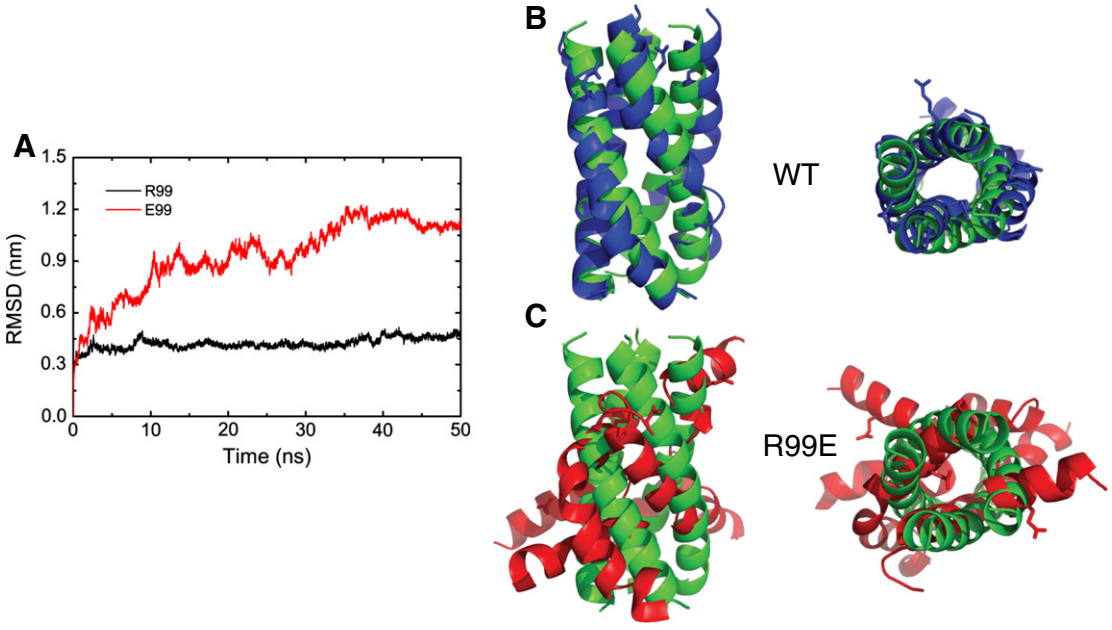

Fig. 6. (A) Time evolution of RMSD against the initial tetrameric model 3 for WT (R99, black) and mutant R99E (E99, red line); (B–C) initial model (green) and representative structures (side and top view) taken after the simulation for WT (blue, B) and mutant R99E (red, C) α3 helix. The structures were obtained by RMSD-based clustering using single-linkage algorithm with a cutoff value of 2.5 Å. Shown structures are the middle structure of the largest cluster.

tendency to form a β-structure, and this was strongly dependent of the protein/lipid ratio (Fig. 5D). Further, whenever the peptide was α-helical, the sample was not amenable to orientation studies as the order was too low. The synthetic α4–α5 peptide (Fig. 5D) did not have the tendency to form a β-structure and it was well inserted in lipid bilayers, with 80% protected residues after H/D exchange, but the amide I and A dichroisms were too low (1.5 ± 0.08 and 2 ± 0.1), and the order parameter was almost zero 0.02 ± 0.03, which again was unsuitable to determine rotational orientations. It is likely that Cry4Ba α5 requires the presence of a full domain I or at least a more extended polypeptide to order properly in the membrane.

One of the paradigms to explain toxicity is through formation of a transmembrane pore [52] mediated by domain I [8], where oligomerization is necessary for toxicity [53], but not sufficient [54,55]. Oligomers have been observed after the toxin binds BBM vesicles [55–57] or synthetic-lipid liposomes [54], using atomic force microscopy (AFM) in model lipid bilayers [58,59], and a clear trimeric form was reported using electron crystallography data obtained from 2D crystals [60]. A "pre-pore" tetrameric oligomer of ~250 kD, that would form after interaction of Cry1 toxins with the cadherin receptor, has also been reported [16,61,62], and has been proposed to be the pore-forming species. In the so-called "umbrella" model [49], only helices α4 and α5 of domain I are inserted into the membrane as an α-helical hairpin [7,63], with the remaining α-helices in domain I parallel to the membrane surface. Mutagenesis and biophysical data indicate that helix α5 is involved in oligomerization, whereas helix α4 is lining the lumen of a putative channel or pore [7]. Mutations at α4 which render the protein non-toxic, or reduce conductance in planar lipid bilayers, do not affect either oligomerization [55,57] or binding to BBM vesicles [64,65]. In contrast, α5 mutations that affect toxicity generally also affect oligomerization [54,55]. Further, synthetic α5 peptides, but not α4, oligomerize in solution as well as in membranes. This paper adds α3 to the list of oligomerizing domain I peptides. Helix α7 may also insert in membranes, as reported previously for Cry3a [49] and Cry4Ba [66]. In the latter paper, it was found that the 27-residue α7 peptide folded as both α and β structures in DMPC membranes, but complete β structure and α-helix were observed in DDPC and DMPG, respectively [66]. In addition, these conformations were found to depend strongly on the protein/lipid ratio, as we found for α5. For DMPC, for example, the proportion of α-helix increased to 90% when the ratio was 1:100, versus a ~65% for a ratio of 1:30. The peptide was only α-helical in anionic DMPG membranes, irrespective of the P/L ratio. Taken together, these results show that the so-called 'umbrella model' may be in fact more complex than previously anticipated, with helices α3, α4, α5 and α7 likely inserted in the lipid bilayer in a concerted mechanism. It has been suggested that α7 may serve as a binding sensor that could initiate the binding of the pore-forming domain to the lipid membrane, facilitating the membrane insertion of the α4–α5 pore-lining hairpin [49]. The model presented herein suggests that α4 would be the main helix lining a hypothetic pore, whereas both α5 and α3 would be involved in the oligomerization of the toxin at the membrane. Recent studies using single molecule fluorescence have shown that *B. thuringiensis* Cry1Aa forms tetramers in lipid bilayers, but substantial amounts of trimers were also observed [18]. Thus the observation of α3 helix tetramerization (herein) and α5 helix trimerization [32] tendencies is significant.

An alternative mechanism for toxicity is derived from observations in insect cells that express the *M. sexta* Cry1Ab toxin receptor Bt-R_1, which show that toxicity originates from sequential activation by the toxin monomer of a cell signaling pathway. This ultimately leads to cell cytoskeleton destabilization [67] after translocation of the toxin through the membrane. Both mechanisms of toxicity require a tendency of at least some of the α-helices in domain I to partition in lipid bilayers. Finally, the possibility that the behavior of these individual helices is different in the context of the complete domain I cannot be neglected.

In summary, our results support a tetrameric interaction of Cry toxins in solution mediated in part by helix α3. Whether this interaction occurs only in solution, in the membrane, or in both environments is still unknown in the absence of more data.

Acknowledgements

This material is based on research/work supported by the Singapore National Research Foundation under CRP Award No. NRF-CRP4-2008-02.

References

[1] N. Crickmore, D.R. Zeigler, J. Feitelson, E. Schnepf, J. Van Rie, D. Lereclus, J. Baum, D.H. Dean, Revision of the nomenclature for the *Bacillus thuringiensis* pesticidal crystal proteins, Microbiol. Mol. Biol. Rev. 62 (1998) 807–813.
[2] H. Hofte, H.R. Whiteley, Insecticidal crystal proteins of *Bacillus thuringiensis*, Microbiol. Rev. 53 (1989) 242–255.
[3] B.R. Lentz, V. Malinin, M.E. Haque, K. Evans, Protein machines and lipid assemblies: current views of cell membrane fusion, Curr. Opin. Struct. Biol. 10 (2000) 607–615.
[4] P. Boonserm, P. Davis, D.J. Ellar, J. Li, Crystal structure of the mosquito-larvicidal toxin Cry4Ba and its biological implications, J. Mol. Biol. 348 (2005) 363–382.
[5] P. Boonserm, D.J. Ellar, J. Li, Crystallization and preliminary X-ray diffraction studies of a mosquito-larvicidal toxin from *Bacillus thuringiensis* subsp. israelensis, Acta Crystallogr. D Biol. Crystallogr. 59 (2003) 591–594.
[6] P. Grochulski, L. Masson, S. Borisova, M. Pusztai-Carey, J.-L. Schwartz, R. Brousseau, M. Cygler, *Bacillus thuringiensis* CryIA(a) insecticidal toxin: crystal structure and channel formation, J. Mol. Biol. 254 (1995) 447–464.
[7] J.L. Schwartz, M. Juteau, P. Grochulski, M. Cygler, G. Prefontaine, R. Brousseau, L. Masson, Restriction of intramolecular movements within the Cry1Aa toxin molecule of *Bacillus thuringiensis* through disulfide bond engineering, FEBS Lett. 410 (1997) 397–402.
[8] F.S. Walters, S.L. Slatin, C.A. Kulesza, L.H. English, Ion channel activity of N-terminal fragments from CryIA(c) delta-endotoxin, Biochem. Biophys. Res. Commun. 196 (1993) 921–926.
[9] A. Lorence, A. Darszon, C. Diaz, A. Lievano, R. Quintero, A. Bravo, Delta-endotoxins induce cation channels in *Spodoptera frugiperda* brush border membranes in suspension and in planar lipid bilayers, FEBS Lett. 360 (1995) 217–222.
[10] R.A. De Maagd, M.S.G. Kwa, H.D. Van Klei, T. Yamamoto, B. Schipper, J.M. Vlak, W.J. Stiekema, D. Bosch, Domain III substitution in *Bacillus thuringiensis* delta-endotoxin CryIA(b) results in superior toxicity for *Spodoptera exigua* and altered membrane protein recognition, Appl. Environ. Microbiol. 62 (1996) 1537–1543.
[11] L. Pardo-Lopez, M. Soberon, A. Bravo, *Bacillus thuringiensis* insecticidal three-domain Cry toxins: mode of action, insect resistance and consequences for crop protection, FEMS Microbiol. Rev. 37 (2013) 3–22.
[12] B.H. Knowles, Mechanism of action of *Bacillus thuringiensis* Insecticidal delta-endotoxins, Adv. Insect Physiol. 24 (1994) 275–308.
[13] M.E. Whalon, B.A. Wingerd, Bt: mode of action and use, Arch. Insect Biochem. Physiol. 54 (2003) 200–211.
[14] S. Swift, A.J. Leger, J. Talavera, L. Zhang, A. Bohm, A. Kuliopulos, Role of the PAR1 receptor 8th helix in signaling: the 7-8-1 receptor activation mechanism, in, J. Biol. Chem. 281 (2006) 4109–4116.
[15] C. Rausell, I. Garcia-Robles, J. Sanchez, C. Munoz-Garay, A.C. Martinez-Ramirez, M.D. Real, A. Bravo, Role of toxin activation on binding and pore formation activity of the *Bacillus thuringiensis* Cry3 toxins in membranes of Leptinotarsa decemlineata (Say), Biochim. Biophys. Acta 1660 (2004) 99–105.
[16] I. Gomez, J. Sanchez, R. Miranda, A. Bravo, M. Soberon, Cadherin-like receptor binding facilitates proteolytic cleavage of helix α-1 in domain I and oligomer pre-pore formation of *Bacillus thuringiensis* Cry1Ab toxin, FEBS Lett. 513 (2002) 242–246.
[17] S. Pacheco, I. Gomez, S.S. Gill, A. Bravo, M. Soberon, Enhancement of insecticidal activity of *Bacillus thuringiensis* Cry1A toxins by fragments of a toxin-binding cadherin correlates with oligomer formation, Peptides 30 (2009) 583–588.
[18] N. Groulx, H. McGuire, R. Laprade, J.L. Schwartz, R. Blunck, Single molecule fluorescence study of the *Bacillus thuringiensis* toxin Cry1Aa reveals tetramerization, J. Biol. Chem. 286 (2011) 42274–42282.
[19] N. Jimenez-Juarez, C. Munoz-Garay, I. Gomez, G. Saab-Rincon, J.Y. Damian-Almazo, S.S. Gill, M. Soberon, A. Bravo, *Bacillus thuringiensis* Cry1Ab mutants affecting oligomer formation are non-toxic to Manduca sexta larvae, J. Biol. Chem. 282 (2007) 21222–21229.
[20] J.D. Li, J. Carroll, D.J. Ellar, Crystal structure of insecticidal delta-endotoxin from *Bacillus thuringiensis* at 2.5 A resolution, Nature 353 (1991) 815–821.
[21] M. Kirouac, V. Vachon, J.F. Noel, F. Girard, J.L. Schwartz, R. Laprade, Amino acid and divalent ion permeability of the pores formed by the *Bacillus thuringiensis* toxins Cry1Aa and Cry1Ac in insect midgut brush border membrane vesicles, Biochim. Biophys. Acta 1561 (2002) 171–179.
[22] J.A.G. Briggs, J. Torres, I.T. Arkin, A new method to model membrane protein structure based on silent amino acid substitutions, Proteins Struct. Funct. Genet. 44 (2001) 370–375.
[23] J. Torres, T.J. Stevens, M. Samso, Membrane proteins: the 'Wild West' of structural biology, Trends Biochem. Sci. 28 (2003) 137–144.
[24] J. Torres, J. Wang, K. Parthasarathy, D.X. Liu, The transmembrane oligomers of coronavirus protein E, Biophys. J. 88 (2005) 1283–1290.
[25] X. Lin, S.M. Tan, S.K.A. Law, J. Torres, Two types of transmembrane homomeric interactions in the integrin receptor family are evolutionarily conserved, Proteins 63 (2006) 16–23.

[26] X. Lin, S.M. Tan, S.K.A. Law, J. Torres, Unambiguous prediction of human integrin transmembrane heterodimer interactions using only homologous sequences, Proteins Struct. Funct. Genet. 65 (2006) 274–279.
[27] S.W. Gan, L. Xin, J. Torres, The transmembrane homotrimer of ADAM 1 in model lipid bilayers, Protein Sci. 16 (2007) 285–292.
[28] S.W. Gan, E. Tan, X. Lin, D. Yu, J. Wang, G.M.-Y. Tan, A. Vararattanavech, C.Y. Yeo, C.H. Soon, T.W. Soong, K. Pervushin, J. Torres, The small hydrophobic protein of the human respiratory syncytial virus forms pentameric ion channels, J. Biol. Chem. 287 (2012) 24671–24689.
[29] A.T. Brunger, P.D. Adams, G.M. Clore, W.L. DeLano, P. Gros, R.W. Grosse-Kunstleve, J. S. Jiang, J. Kuszewski, M. Nilges, N.S. Pannu, R.J. Read, L.M. Rice, T. Simonson, G.L. Warren, Crystallography & NMR system: a new software suite for macromolecular structure determination, Acta Crystallogr. D Biol. Crystallogr. 54 (1998) 905–921.
[30] P.D. Adams, I.T. Arkin, D.M. Engelman, A.T. Brunger, Computational searching and mutagenesis suggest a structure for the pentameric transmembrane domain of phospholamban, Nat. Struct. Biol. 2 (1995) 154–162.
[31] J. Torres, J.A. Briggs, I.T. Arkin, Contribution of energy values to the analysis of global searching molecular dynamics simulations of transmembrane helical bundles, Biophys. J. 82 (2002) 3063–3071.
[32] J. Torres, X. Lin, P. Boonserm, A trimeric building block model for Cry toxins in vitro ion channel formation, Biochim. Biophys. Acta 1778 (2008) 392–397.
[33] W.L. Jorgensen, J. Chandrasekhar, J.D. Madura, R.W. Impey, M.L. Klein, Comparison of simple potential functions for simulating liquid water, J. Chem. Phys. 79 (1983) 926–935.
[34] D. Van der Spoel, E. Lindahl, B. Hess, G. Groenhof, A.E. Mark, H.J.C. Berendsen, GROMACS: fast, flexible, and free, J. Comput. Chem. 26 (2005) 1701–1718.
[35] B. Hess, H. Bekker, H.J.C. Berendsen, J. Fraaije, LINCS: a linear constraint solver for molecular simulations, J. Comput. Chem. 18 (1997) 1463–1472.
[36] U. Essmann, L. Perera, M.L. Berkowitz, T. Darden, H. Lee, L.G. Pedersen, A smooth particle mesh Ewald method, J. Chem. Phys. 103 (1995) 8577–8593.
[37] G. Bussi, D. Donadio, M. Parrinello, Canonical sampling through velocity rescaling, J. Chem. Phys. 126 (2007) 014101–014107.
[38] R. Koradi, M. Billeter, K. Wuthrich, MOLMOL: a program for display and analysis of macromolecular structures, J. Mol. Graph. 14 (1996) 51–55 (29–32).
[39] J. Torres, P.D. Adams, I.T. Arkin, Use of a new label, $^{13}C{=}{=}^{18}O$, in the determination of a structural model of phospholamban in a lipid bilayer. Spatial restraints resolve the ambiguity arising from interpretations of mutagenesis data, J. Mol. Biol. 300 (2000) 677–685.
[40] D.A. Wellings, E. Atherton, Standard FMOC protocols, Methods Enzymol. 289 (1997) 44–67.
[41] I.T. Arkin, K.R. MacKenzie, A.T. Brunger, Site-directed dichroism as a method for obtaining rotational and orientational constraints for oriented polymers, J. Am. Chem. Soc. 119 (1997) 8973–8980.
[42] C. Combet, C. Blanchet, C. Geourjon, G. Deleage, NPS@: network protein sequence analysis, Trends Biochem. Sci. 25 (2000) 147–150.
[43] G.G. Kochendoerfer, D. Salom, J.D. Lear, R. Wilk-Orescan, S.B. Kent, W.F. DeGrado, Total chemical synthesis of the integral membrane protein influenza A virus M2: role of its C-terminal domain in tetramer assembly 1, Biochemistry 38 (1999) 11905–11913.
[44] R. Li, C.R. Babu, J.D. Lear, A.J. Wand, J.S. Bennett, W.F. DeGrado, Oligomerization of the integrin αIIbβ3: roles of the transmembrane and cytoplasmic domains, Proc. Natl. Acad. Sci. U. S. A. 98 (2001) 12462–12467.
[45] T.M. Laue, W.F. Stafford III, Modern applications of analytical ultracentrifugation, Annu. Rev. Biophys. Biomol. Struct. 28 (1999) 75–100.
[46] P. Schuck, On the analysis of protein self-association by sedimentation velocity analytical ultracentrifugation, Anal. Biochem. 320 (2003) 104–124.
[47] D. Marsh, Quantitation of secondary structure in ATR infrared spectroscopy, Biophys. J. 77 (1999) 2630–2637.
[48] E.J. McGhie, P.J. Hume, R.D. Hayward, J. Torres, V. Koronakis, Topology of the Salmonella invasion protein SipB in a model bilayer, Mol. Microbiol. 44 (2002) 1309–1321.
[49] E. Gazit, P. La Rocca, M.S.P. Sansom, Y. Shai, The structure and organization within the membrane of the helices composing the pore-forming domain of *Bacillus thuringiensis* delta-endotoxin are consistent with an "umbrella-like" structure of the pore, Proc. Natl. Acad. Sci. U. S. A. 95 (1998) 12289–12294.
[50] C. Rodriguez-Almazan, L.E. Zavala, C. Munoz-Garay, N. Jimenez-Juarez, S. Pacheco, L. Masson, M. Soberon, A. Bravo, Dominant negative mutants of bacillus thuringiensis Cry1Ab toxin function as anti-toxins: demonstration of the role of oligomerization in toxicity, PLoS ONE 4 (2009).
[51] A.L. Stouffer, C. Ma, L. Cristian, Y. Ohigashi, R.A. Lamb, J.D. Lear, L.H. Pinto, W.F. DeGrado, The interplay of functional tuning, drug resistance, and thermodynamic stability in the evolution of the M2 proton channel from the influenza A virus, Structure 16 (2008) 1067–1076.
[52] B.H. Knowles, D.J. Ellar, Colloid-osmotic lysis is a general feature of the mechanism of action of *Bacillus thuringiensis* d-endotoxins with different insect specificity, Biochim. Biophys. Acta Gen. Subj. 924 (1987) 509–518.
[53] M. Soberon, R.V. Perez, M.E. Nunez-Valdez, A. Lorence, I. Gomez, J. Sanchez, A. Bravo, Evidence for intermolecular interaction as a necessary step for pore-formation activity and toxicity of *Bacillus thuringiensis* Cry1Ab toxin, FEMS Microbiol. Lett. 191 (2000) 221–225.
[54] S. Likitvivatanavong, G. Katzenmeier, C. Angsuthanasombat, Asn_{183} in a5 is essential for oligomerisation and toxicity of the *Bacillus thuringiensis* Cry4Ba toxin, Arch. Biochem. Biophys. 445 (2006) 46–55.
[55] A.I. Aronson, C.X. Geng, L. Wu, Aggregation of *Bacillus thuringiensis* Cry1A toxins upon binding to target insect larval midgut vesicles, Appl. Environ. Microbiol. 65 (1999) 2503–2507.
[56] N.J. Tigue, J. Jacoby, D.J. Ellar, The alpha-helix 4 residue, Asn135, is involved in the oligomerization of Cry1Ac1 and Cry1Ab5 *Bacillus thuringiensis* toxins, Appl. Environ. Microbiol. 67 (2001) 5715–5720.
[57] A.S.M. Kumar, A.I. Aronson, Analysis of mutations in the pore-forming region essential for insecticidal activity of a *Bacillus thuringiensis* delta-endotoxin, J. Bacteriol. 181 (1999) 6103–6107.
[58] T. Puntheeranurak, C. Stroh, R. Zhu, C. Angsuthanasombat, P. Hinterdorfer, Structure and distribution of the *Bacillus thuringiensis* Cry4Ba toxin in lipid membranes, Ultramicroscopy 105 (2005) 115–124.
[59] V. Vie, N. Van Mau, P. Pomarede, C. Dance, J.L. Schwartz, R. Laprade, R. Frutos, C. Rang, L. Masson, F. Heitz, C. Le Grimellec, Lipid-induced pore formation of the *Bacillus thuringiensis* Cry1Aa insecticidal toxin, J. Membr. Biol. 180 (2001) 195–203.
[60] P. Ounjai, V.M. Unger, F.J. Sigworth, C. Angsuthanasombat, Two conformational states of the membrane-associated *Bacillus thuringiensis* Cry4Ba delta-endotoxin complex revealed by electron crystallography: Implications for toxin-pore formation, Biochem. Biophys. Res. Commun. 361 (2007) 890–895.
[61] C. Rausell, C. Munoz-Garay, R. Miranda-CassoLuengo, I. Gomez, E. Rudino-Pinera, M. Soberon, A. Bravo, Tryptophan spectroscopy studies and black lipid bilayer analysis indicate that the oligomeric structure of Cry1Ab toxin from *Bacillus thuringiensis* is the membrane-insertion intermediate, Biochemistry 43 (2004) 166–174.
[62] C. Rausell, L. Pardo-Lopez, J. Sanchez, C. Munoz-Garay, C. Morera, M. Soberon, A. Bravo, Unfolding events in the water-soluble monomeric Cry1Ab toxin during transition to oligomeric pre-pore and membrane-inserted pore channel, J. Biol. Chem. 279 (2004) 55168–55175.
[63] D. Gerber, Y. Shai, Insertion and organization within membranes of the delta-endotoxin pore-forming domain, helix 4-loop-helix 5, and inhibition of its activity by a mutant helix 4 peptide, J. Biol. Chem. 275 (2000) 23602–23607.
[64] L. Masson, B.E. Tabashnik, L. Yong-Biao, R. Brousseau, J.-L. Schwartz, Helix 4 of the *Bacillus thuringiensis* Cry1Aa toxin lines the lumen of the ion channel, J. Biol. Chem. 274 (1999) 31996–32000.
[65] V. Vachon, G. Prefontaine, C. Rang, F. Coux, M. Juteau, J.L. Schwartz, R. Brousseau, R. Frutos, R. Laprade, L. Masson, Helix 4 mutants of the *Bacillus thuringiensis* insecticidal toxin Cry1Aa display altered pore-forming abilities, Appl. Environ. Microbiol. 70 (2004) 6123–6130.
[66] K. Tiewsiri, W.B. Fischer, C. Angsuthanasombat, Lipid-induced conformation of helix 7 from the pore-forming domain of the *Bacillus thuringiensis* Cry4Ba toxin: implications for toxicity mechanism, Arch. Biochem. Biophys. 482 (2009) 17–24.
[67] X. Zhang, M. Candas, N.B. Griko, R. Taussig, L.A. Bulla Jr., A mechanism of cell death involving an adenylyl cyclase/PKA signaling pathway is induced by the Cry1Ab toxin of *Bacillus thuringiensis*, Proc. Natl. Acad. Sci. U. S. A. 103 (2006) 9897–9902.